Molecular Crystals and Liquid Crystals Science and Technology. Section A. Molecular Crystals and Liquid Crystals
Publication details, including instructions for authors and subscription information:
http://www.tandfonline.com/loi/gmcl19

Flow of a Nematic Liquid Crystal Around a Sphere

H. Heuer [a] , H. Kneppe [a] & F. Schneider [a]
[a] Physikalische Chemie, Universität Siegen, 5900, Siegen, Germany
Version of record first published: 24 Sep 2006.

To cite this article: H. Heuer , H. Kneppe & F. Schneider (1992): Flow of a Nematic Liquid Crystal Around a Sphere, Molecular Crystals and Liquid Crystals Science and Technology. Section A. Molecular Crystals and Liquid Crystals, 214:1, 43-61

To link to this article: http://dx.doi.org/10.1080/10587259208037281

Mol. Cryst. Liq. Cryst., 1992, Vol. 214, pp. 43–61
Reprints available directly from the publisher
Photocopying permitted by license only

Printed in the United States of America

Flow of a Nematic Liquid Crystal around a Sphere

H. HEUER, H. KNEPPE and F. SCHNEIDER
Physikalische Chemie, Universität Siegen, 5900 Siegen, Germany

(Received August 6, 1991)

The flow of an incompressible nematic liquid crystal around a sphere is studied for arbitrary angles between the director and the flow velocity at infinite distances. We assume low Reynolds numbers and a fixed director orientation for the calculation on the basis of the Leslie-Ericksen equations. The calculations are performed with a finite difference method which is a combination of the artificial compressibility method for the pressure determination and a simultaneous over-relaxation (SOR, SSOR) for the solution of the momentum equations. We find strong differences in the stream line patterns of a usual liquid crystal as compared with those of an isotropic liquid if the direction of the director is perpendicular to the flow velocity. The force on the sphere is calculated. Equations are presented which allow the determination of the force for a broad range of anisotropies of the viscosity coefficients. The falling direction of a sphere deviates from the direction of gravity by 25° for a liquid crystal with $\eta_1 : \eta_2 : \eta_3 = 10:1:3$ if the angle between director and direction of gravity is 58°.

I. INTRODUCTION

Recently, we have studied the flow of a nematic liquid crystal around a sphere in the axisymmetrical case,[1] i.e., the orientation of the director is parallel to the flow velocity v_∞ at infinite distance from the sphere. It turned out that it is possible to treat the problem by means of an analytical method if the Leslie coefficient α_1 is neglected and if a fixed director orientation is assumed. In order to achieve the general solution with arbitrary angles between director and flow velocity v_∞ it is necessary to know the solution for a director orientation perpendicular to the flow velocity v_∞.

This paper describes a finite difference method for the evaluation of the flow pattern, the pressure and the force on the sphere for the perpendicular case. Furthermore, the solution for the parallel case is generalized for $\alpha_1 \neq 0$.

II. GENERAL REMARKS

As in paper I[2] and II,[1] we assume a flow with low Reynolds numbers, an incompressible nematic liquid crystal with a fixed director orientation ($\boldsymbol{n}$ = const) and a weak anchoring of the director at the surface of the sphere. In paper II, we

presented a series representation for the velocities and the pressure for the axisymmetrical case ($v_\infty \| n$) under the assumption that the Leslie coefficient α_1 can be neglected. In this paper, we want to study the general case with $\alpha_1 \neq 0$ and an arbitrary angle ψ between the velocity v_∞ at infinite distance and the director n. As the momentum equations and the continuity equation are linear, the solution for an arbitrary angle ψ can be found by a superposition of the two solutions for $\psi = 0$ and 90°. Thus, only these two cases have to be studied.

III. AXISYMMETRICAL CASE

Hydrodynamic Equations

The momentum equations for the case $n \| z$ have already been derived from the Leslie-Ericksen equations[3,4] in paper II:

$$-p'_{,x} + \eta_3 \Delta v_x + (\eta_1 - \eta_3)(v_{x,zz} - v_{z,zx}) = 0 \tag{1}$$

$$-p'_{,y} + \eta_3 \Delta v_y + (\eta_1 - \eta_3)(v_{y,zz} - v_{z,zy}) = 0 \tag{2}$$

$$-p'_{,z} + \eta_2 \Delta v_z + \alpha_1 v_{z,zz} = 0 \tag{3}$$

with

$$p' = p - \alpha_5 v_{z,z} \tag{4}$$

A comma preceeding a suffix denotes a partial differentiation with respect to the following coordinate. η_1, η_2, and η_3 are the shear viscosity coefficients; α_1 and α_5 are Leslie coefficients. A more detailed description of the coefficients is given in paper II. These equations are transformed in the axisymmetrical case $v_\infty \| n \| z$ into cylindrical coordinates (ρ, z)

$$-p'_{,\rho} + \eta_1[v_{\rho,\rho\rho} + v_{\rho,zz} + v_{\rho,\rho}/\rho - v_\rho/\rho^2] = 0 \tag{5}$$

$$-p'_{,z} + \eta_2[v_{z,\rho\rho} + (1 + \alpha_1/\eta_2)v_{z,zz} + v_{z,\rho}/\rho] = 0 \tag{6}$$

$$v_{z,z} + v_{\rho,\rho} + v_\rho/\rho = 0 \tag{7}$$

where the last equation is the continuity equation.

The director orientation, the existence of a boundary condition at $r = \infty$ and the symmetry of the boundary conditions

$$v_{r=1} = (0, 0, 0) \quad \text{and} \quad v_{r=\infty} = (0, 0, v_\infty)$$

suggest a further transformation into spherical coordinates with a reciprocal radius ξ as variable

$$\xi = 1/\sqrt{\rho^2 + z^2}; \qquad \tan\vartheta = \rho/z \tag{8}$$

The corresponding transformation of the velocity components would lead to rather complex equations. Therefore, the velocity components v_z and v_ρ were retained. Furthermore, we introduce the dimensionless quantities

$$p'/\eta_2 v_\infty R^{-1} \to p'; \qquad v_i/v_\infty \to v_i; \qquad \xi/R^{-1} \to \xi$$

where R is the radius of the sphere. Equation (5) to (7) become

$$\xi \sin\vartheta\, p'_{,\xi} - \cos\vartheta\, p'_{,\vartheta} + \frac{\eta_1}{\eta_2}\xi(\partial^2_\vartheta + \xi^2\partial^2_\xi + \cot\vartheta\, \partial_\vartheta - 1/\sin^2\vartheta)v_\rho = 0 \quad (9)$$

$$\xi \cos\vartheta\, p'_{,\xi} + \sin\vartheta\, p'_{,\vartheta} + \xi(\partial^2_\vartheta + \xi^2\partial^2_\xi + \cot\vartheta\, \partial_\vartheta)v_z + \frac{\alpha_1}{\eta_2}\xi[\sin^2\vartheta\, \partial^2_\vartheta + \xi^2 \cos^2\vartheta\, \partial^2_\xi + \sin 2\vartheta(\xi\, \partial_{\vartheta\xi} + \partial_\vartheta) + \xi(2 - 3\sin^2\vartheta)\partial_\xi]v_z = 0 \quad (10)$$

$$\xi[(-\xi \sin\vartheta\, \partial_\xi + \cos\vartheta\, \partial_\vartheta + 1/\sin\vartheta)v_\rho - (\xi \cos\vartheta\, \partial_\xi + \sin\vartheta\, \partial_\vartheta)v_z] = 0 \quad (11)$$

The force on the sphere can be taken over from paper II

$$F^* = \frac{F}{6\pi\eta_2 R v_\infty} = \frac{2}{3}\int_0^{\pi/2} [-\cos\vartheta\, p' + 1 + \frac{\alpha_1}{\eta_2}\cos^2\vartheta \sin\vartheta\, v_{\vartheta,\xi}] \sin\vartheta\, d\vartheta \quad (12)$$

The use of cartesian coordinates instead of spherical coordinates for the velocity component would lead to a longer equation.

Finite Difference Equations and Numerical Solution

Equations (9) and (10) differ from the corresponding equations for isotropic fluids in cartesian coordinates by the first derivatives of the velocities and by the pressure derivatives in both directions. Equation (11) contains both derivatives for each velocity component. This leads to some difficulties when using the staggered (MAC) grid introduced by Harlow and Welsh.[5] In our case, a grid is advantageous in which only the pressure is staggered. Figure 1 shows a quadrant of this grid in real and reciprocal space for a small number of nodes. The momentum equations are discretized at the velocity points. Centered differences were used for the first and second derivatives of the velocities. Derivatives of the pressure at these points were obtained from the four nearest pressure points, e.g.

$p_{,\xi}(i, j)$:

$$\frac{p\left(i-\frac{1}{2}, j+\frac{1}{2}\right) + p\left(i+\frac{1}{2}, j+\frac{1}{2}\right) - p\left(i-\frac{1}{2}, j-\frac{1}{2}\right) - p\left(i+\frac{1}{2}, j-\frac{1}{2}\right)}{2\Delta\xi} \quad (13)$$

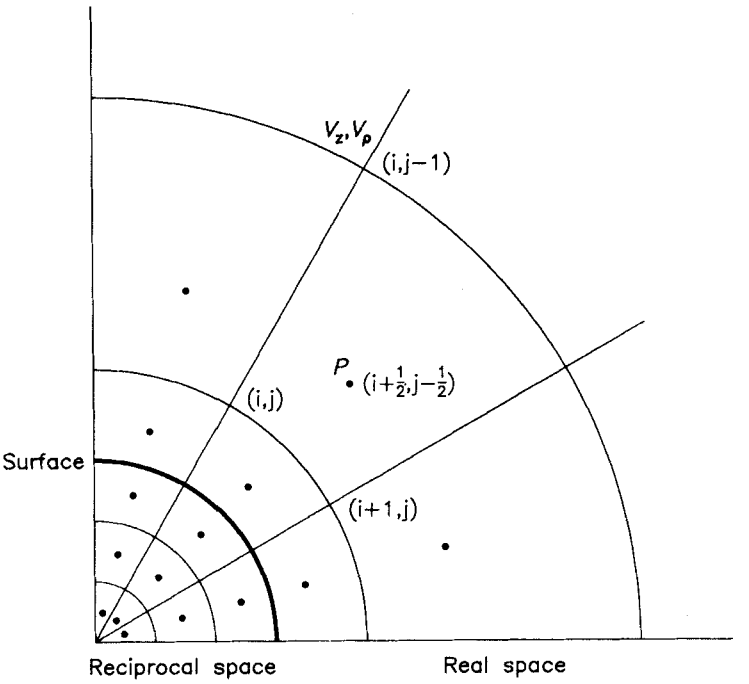

FIGURE 1 Grid for the numerical calculation. The first term in the parentheses denotes the point number in ϑ and the second in ξ direction.

Both difference equations are second-order accurate approximations of the differential equations. The continuity equation was discretized at the pressure points using the four nearest velocities for each derivative similar to Equation (13). v_ρ in the term $v_\rho/\sin\vartheta$ was calculated from the mean of the four nearest v_ρ values and is the only term which is first-order accurate. The symmetry of the problem allows to reduce the area for the calculation to a quadrant. Velocities and pressures outside of the quadrant which are needed for the calculation at the border of the quadrant are found by symmetry operations from the inside values. The v_z equation at $\vartheta = 0$ has to be modified as it contains $\cot\vartheta$. For $\vartheta = 0$, $\cot\vartheta\ \partial v_z/\partial\vartheta$ can be replaced by $\partial^2 v_z/\partial\vartheta^2$ and the equation becomes

$$p_{,\xi} + [2\partial_\vartheta^2 + \xi^2\partial_\xi^2 + \frac{\alpha_1}{\eta_2}(\xi^2\partial_\xi^2 + 2\xi\partial_\xi)]v_z = 0 \tag{14}$$

In paper I, we used the artificial compressibility method[6,7] for the solution of the difference equations. This method is simple but it converges very slowly especially in the perpendicular case which will be discussed later on. This is due to the fact that the time dependent equations used in this method are principally wave equations containing a small damping term. This leads to temporal oscillations which

are nearly undamped. We have, therefore, only retained the pressure generation of the artificial compressibility method

$$\frac{\partial p}{\partial t} = -c^2 \operatorname{div} v \tag{15}$$

but have used the successive over-relaxation (SOR) method for the determination of the velocities from the momentum equations. For large systems, the convergence to the steady state increased by several orders of magnitude. The symmetric SOR method (SSOR) did not lead to a further increase of the convergence. Therefore, Equations (9) and (10) were discretized as described and solved with the SOR method. Every SOR cycle was followed by a pressure correction cycle according to

$$\Delta p = -\beta \operatorname{div} v \tag{16}$$

where div v was replaced by the discretized form of Equation (11). Large over-relaxation parameters and pressure correction factors β lead to the fastest convergence. However, an upper limit for both quantities is given by the demand for numerical stability.

The force on the sphere was determined with the aid of Equation (12) using a numerical integration.

Results

A comparison between the velocities, pressures and forces calculated with the numerical method with $\alpha_1 = 0$ and that calculated with the analytical method (paper II) showed that the values agree within about 0.1% for a grid with 39 points in ξ and ϑ direction. The velocities, pressures and forces converge with the node numbers $N_\xi = N_\vartheta = N \to \infty$ towards the values determined with the analytical method. This is shown in Figure 2 for the force. Obviously, the method is second-order accurate i.e., the calculation of the term $v_\rho/\sin\vartheta$ with a first-order accurate method plays only a minor role.

Furthermore, we studied the influence of α_1 on the dimensionless force which is in a first order perturbation (paper II)

$$F^* = 1 + \frac{2}{15}\frac{\alpha_1}{\eta} \tag{17}$$

for a liquid crystal with equal shear viscosities $\eta_1 = \eta_2 = \eta$. The numerical calculation on a grid with 51 points in both directions leads for small α_1/η values ($\alpha_1/\eta < 1$) to a linear dependence corresponding to Equation (17) with a slope of 0.113 instead of $2/15 = 0.1\bar{3}$.

The numerical calculations show that the second term in the force equation of paper II for the general case $\eta_1 \neq \eta_2$

$$F^* = A(\gamma) + \frac{\alpha_1}{\eta_2} B(\gamma) \tag{18}$$

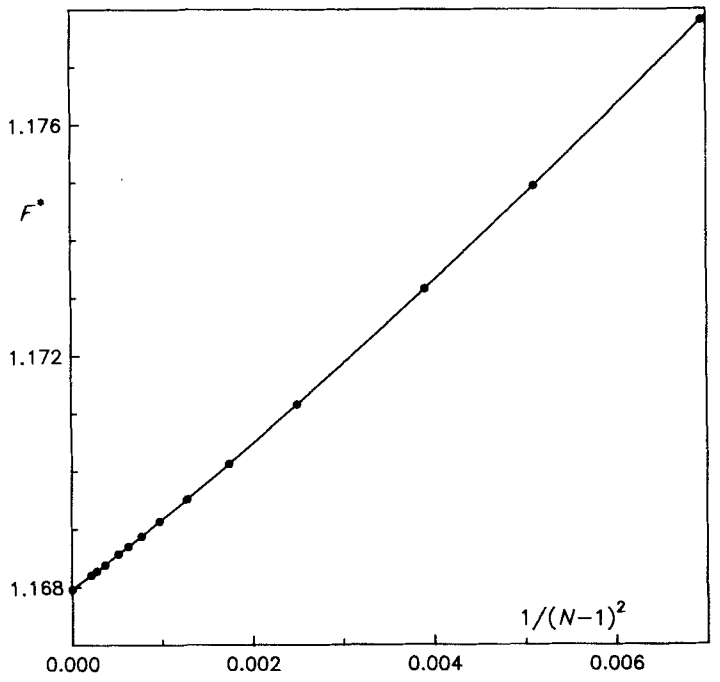

FIGURE 2 Numerically determined force F^* on the sphere for a viscosity coefficient ratio $\eta_1/\eta_2 = 2$ and $\alpha_1 = 0$ as a function of $1/(N-1)^2$ where N is the number of nodes in ξ and ϑ direction. The point at $1/(N-1)^2 = 0$ was calculated by means of Equation (18).

with

$$A(\gamma) = \frac{2}{3}\frac{\gamma\sqrt{|\gamma|/(1+\gamma)}}{\sqrt{|\gamma|(1+\gamma)} - \operatorname{acos}\sqrt{1+\gamma}} \tag{19}$$

$$B(\gamma) = \frac{2}{3}\left(\frac{1}{\gamma} + \frac{1}{3} + \frac{2\operatorname{asin}\sqrt{|\gamma|}}{3(\operatorname{asin}\sqrt{|\gamma|} - \sqrt{|\gamma|(1+\gamma)})}\right) \tag{20}$$

$$\gamma = \frac{\eta_1 - \eta_1}{\eta_1} \tag{21}$$

$$\operatorname{acos}\sqrt{1+\gamma} = \begin{cases} \operatorname{Arch}\sqrt{1+\gamma} & \text{for} \quad \gamma > 0 \\ \arccos\sqrt{1+\gamma} & \text{for} \quad \gamma < 0 \end{cases} \tag{22}$$

and asin analogously is about 15% too small. Due to the small influence of the second term, the precision for the calculation of force is considerably better. Nevertheless, we have improved the formula empirically in the following way. In order

to avoid the main error of the numerical calculation, we used numerically determined values for $F^*(\alpha_1 = 0)$ instead of $A(\gamma)$ and calculated

$$\frac{F^* - F^*(\alpha_1 = 0)}{\frac{\alpha_1}{\eta_2}}$$

for a large number of α_1/η_2 and η_1/η_2 values. The complicated function $B(\gamma)$ can be replaced for the interesting γ values by $1/(b + c\sqrt{\eta_1/\eta_2})$. A fit of an optimized function in α_1/η_2 and η_1/η_2 led to

$$F^* = A(\gamma) + a\frac{\alpha_1}{\eta_2}\frac{C(\eta_1/\eta_2)}{\frac{\alpha_1}{\eta_2} + C^2(\eta_1/\eta_2)} \tag{23}$$

with

$$C(\eta_1/\eta_2) = 1.80599 + 2.10289\sqrt{\eta_1/\eta_2}; \quad a = 0.44627$$

which describes the dependence on α_1/η_2 within .2% for $0.5 < \eta_1/\eta_2 < 10$ and $-0.5 < \alpha_1/\eta_2 < 1.0$.

The influence of α_1 on the flow pattern is invisible for α_1/η_2 values of usual nematic liquid crystals ($\alpha_1/\eta_2 < 1$). Considerably larger α_1 values (e.g. $\alpha_1/\eta_2 = 40$) lead to a smoother flow pattern as compared with $\alpha_1 = 0$ (Figure 3). This is due to the fact that a flow direction in which α_1 becomes effective, i.e. at an angle of about 45° to the z axis, is avoided.

IV. PERPENDICULAR CASE

Hydrodynamic Equations

For the perpendicular case $\psi = 90°$, we use the following configuration

$$\boldsymbol{v}_\infty \parallel z \quad \text{and} \quad \boldsymbol{n} \parallel x$$

This configuration is advantageous for the numerical calculations, but the solution has to be rotated by 90° for a superposition with the axisymmetrical case. The momentum equations for this case are obtained from Equation (1) to (3) by a cyclic rotation of the coordinates. Introduction of the dimensionless quantities

$$p/\eta_3 v_\infty R^{-1} \to p; \quad v_i/v_\infty \to v_i; \quad x/R \to x; \quad y/R \to y; \quad z/R \to z$$

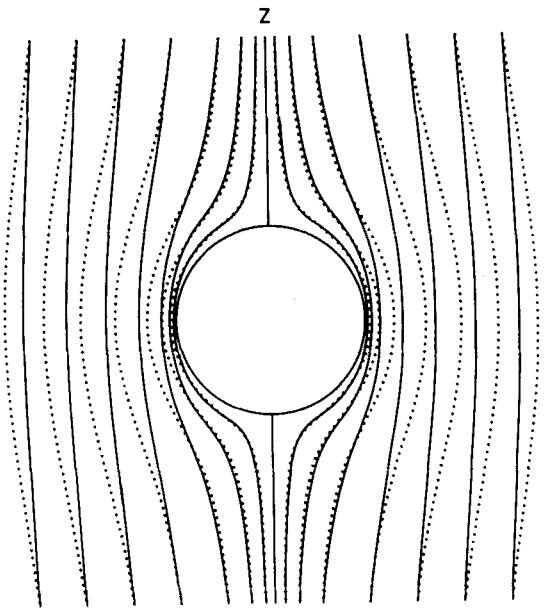

FIGURE 3 Axisymmetrical stream line pattern for the flow of a nematic liquid crystal with $\eta_1 = \eta_2$ and $\alpha_1/\eta_2 = 40$(—) and of an isotropic liquid (· · · ·) around a fixed sphere. The director orientation and the flow velocity v_∞ at infinite distance are parallel to the z axis.

leads to

$$-p''_{,x} + \frac{\eta_2}{\eta_3}\Delta v_x + \left(\frac{\alpha_1}{\eta_3} + \frac{\eta_1 - \eta_3}{\eta_3}\right) v_{x,xx} = 0 \tag{24}$$

$$-p''_{,y} + \Delta v_y + \frac{\eta_1 - \eta_3}{\eta_3} v_{y,xx} = 0 \tag{25}$$

$$-p''_{,z} + \Delta v_z + \frac{\eta_1 - \eta_3}{\eta_3} v_{z,xx} = 0 \tag{26}$$

with

$$p'' = p + \left(-\frac{\alpha_5}{\eta_3} + \frac{\eta_1 - \eta_3}{\eta_3}\right) v_{x,x} \tag{27}$$

The definition of the dimensionless quantities was changed as compared with the axisymmetrical case, as the flow pattern and the force on the sphere are mainly determined by the viscosity coefficient η_3.

As in the axisymmetrical case, these equations were transformed into spherical coordinates (ξ,ϕ,ϑ) with the reciprocal radius ξ

$$\xi = 1/\sqrt{x^2 + y^2 + z^2}; \qquad \tan\phi = y/x; \qquad \tan\vartheta = \sqrt{x^2 + y^2}/z \tag{28}$$

The cartesian velocity components were retained. The derivatives in the reciprocal spherical coordinate system are given in the appendix.

The differential of the force component in z direction on the sphere is in dimensional form

$$dF_z = \sigma_{zx}\, dS_x + \sigma_{zy} dS_y + \sigma_{zz} dS_z$$

$$= (\cos\phi \sin\vartheta\, \sigma_{zx} + \sin\phi \sin\vartheta\, \sigma_{zy} + \cos\vartheta\, \sigma_{zz}) dS_r \quad (29)$$

where the dS_i are the surface elements on the sphere. The tensor components σ_{ij} have to be calculated from the Leslie-Ericksen equations for this particular case

$$\sigma_{zx} = \frac{\alpha_2 + \alpha_4 + \alpha_5}{2} v_{x,z} + \frac{-\alpha_2 + \alpha_4 + \alpha_5}{2} v_{z,x}$$

$$\sigma_{zy} = \frac{\alpha_4}{2}(v_{z,y} + v_{y,z}) \quad (30)$$

$$\sigma_{zz} = -p + \alpha_4 v_{z,z} = -p'' + (\alpha_5 - \eta_1 + \eta_3) v_{x,x} + \alpha_4 v_{z,z}$$

Introduction of reciprocal spherical coordinates, insertion into Equation (29) and integration leads to

$$F^* = \frac{F}{6\pi\eta_3 R\, v_\infty} = \frac{4}{3\pi} \int_{\phi=0}^{\pi/2} \int_{\vartheta=0}^{\pi/2} \Bigg[-\sin\vartheta \cos\vartheta\, p''$$

$$+ \left(1 + \frac{\eta_1 - \eta_3}{\eta_3} \sin^2\vartheta \cos^2\phi\right) \sin^2\vartheta\, v_{\vartheta,\xi} \Bigg] d\vartheta\, d\phi \quad (31)$$

Finite Difference Equations and Numerical Solution

The numerical procedure was the same as in the axisymmetrical case, i.e. the SSOR method (which is somewhat faster in the convergence than the SOR method) for the solution of the momentum equations and a pressure generation from the continuity equation according to Equation (16).

At first, we have tried to use a grid which is a 3-dimensional analogue to the axisymmetrical case, i.e., a grid in which the velocity components are defined on the nodes and the pressure points are staggered. The numerical calculation on this grid led to strong spatial oscillations of the pressure. This is due to the following effect. The first derivatives of the pressure in the momentum equations are calculated from the difference of two mean values over four pressure points. Although these mean values and the corresponding derivatives are correct, the single pressure values can oscillate.

We have, therefore, used a primitive grid in which the velocity components and

the pressure are defined on the nodes. The spatial oscillation of the pressure can be suppressed with a technique to be described later on. The symmetry of the problem allows to reduce the space for the calculation to an octant. Centered differences were used for the first and second derivatives at the nodes inside of the octant. The following quantities are known (value 0 or 1) or have to be calculated (cal) at the surface of the octant for a fixed sphere in a moving liquid crystal.

	$\vartheta = 0$	$\vartheta = \pi/2$	$\phi = 0$	$\phi = \pi/2$	$\xi = 0$	$\xi = 1$
v_x	0	0	cal	0	0	0
v_y	0	0	0	cal	0	0
v_z	cal	cal	cal	cal	1	0
p''	cal	0	cal	cal	0	cal

Centered differences could also be used for the unknown quantities at $\phi = 0$, $\pi/2$ and at $\vartheta = \pi/2$ if the necessary nodes outside of the octant had been added and determined by symmetry from the values at inner nodes. For $\xi = 1$, we used unsymmetrical derivatives in the continuity equation. A modified v_z equation had to be used for $\vartheta = 0$ because of the $\sin^{-2}\vartheta$ and the $\cot\vartheta$ terms. The v_z equation becomes in the limit $\vartheta \to 0$

$$p''_{,\xi} + (\xi^2\partial_\xi^2 + 2\partial_\vartheta^2(\phi = \pi/4))v_z + \frac{\eta_1 - \eta_3}{\eta_3}(\partial_\vartheta^2(\phi = 0) - \xi\partial_\xi)v_z = 0 \quad (32)$$

This equation was discretized using centered differences.

The determination of the pressure from the continuity equation with a modified form for $\vartheta = 0$ led to strong pressure oscillations as a function of ϑ and to small oscillations as a function of ξ whereas the pressure was a smooth function of ϕ. Although the pressure grids are coupled at the boundaries, the different numerical differentiations for $\vartheta = 0$ and $\neq 0$ as well as $\xi = 1$ and $\neq 1$ lead to this oscillation. Therefore, the pressure at $\vartheta = 0$ was determined by an interpolation (!) with an error $O(\Delta\vartheta^4)$ from the two nearest nodes according to $p''_0 = (4p''_1 - p''_2)/3$ and a determination of the mean over all ϕ values. This coupling of the pressure grids completely avoids the pressure oscillation as a function of ϑ. The small oscillation as a function of ξ was removed after the numerical solution of the differential equations by an integration of the correct pressure derivatives $\partial p''/\partial\xi$ from $p'' = 0$ at $\xi = 0$ over ξ. Using different centered differences in the first and the second half of each integration intervall we find

$$\bar{p}''_i = (p''_{i-1} + 2p''_i + p''_{i+1})/4 \quad (33)$$

The smoothed pressure values $\bar{p}''$ were used for the determination of the force on the sphere by a numerical integration of Equation (31).

The introduction of the modified pressure p'' leads to a difficulty if $\eta_1 - \eta_3 + \eta_2 + \alpha_1 < 0$. In this case, Equation (24) is of the hyperbolic type and the over-relaxation method becomes numerically unstable. As this case is not of any practical interest, we did not try to find a suitable method for the calculation in this case.

The real pressure p is calculated from the modified pressure p'' with the aid of Equation (27) and (A1). On the sphere, it becomes

$$p = p'' + \left(-\frac{\alpha_5}{\eta_3} + \frac{\eta_1 - \eta_3}{\eta_3} \right) \cos\phi \sin\vartheta \, v_{x,\xi} \tag{34}$$

Results

In the following, we shall discuss two series of calculations which show the influence of two different types of anisotropies on the flow patterns, the pressure and the force on the sphere. Figure 4 shows which of the viscosity coefficients are effective near the surface of the sphere in the x, z and y, z plane, respectively. The two cases studied are:

$$\text{Case I:} \quad \eta_1, \quad \eta_2 = \eta_3$$

$$\text{Case II:} \quad \eta_1 = \eta_2, \quad \eta_3$$

Case I shows the influence of the anisotropy within the x, y plane; Case II the influence of different viscosities in the x, z and the y, z plane. The following stream line patterns (Figures 5 and 6) show these cases for a coefficient ratio of 5 (Case I: $\eta_1/\eta_3 = 5$, $\eta_2/\eta_3 = 1$; Case II: $\eta_1/\eta_3 = \eta_2/\eta_3 = 5$) in a cylinder projection (z, ϕ coordinates) and in an x, y projection. All stream lines are beginning at $z = 3$ and $\rho = 0.25$.

In the axisymmetrical case, the stream line patterns are mainly determined by the boundary condition at the surface of the sphere and the continuity equation and the difference between an isotropic and an anisotropic liquid is rather small. In the perpendicular case, however, we find strong differences. Due to the differences in the effective viscosity as a function of ϕ, the stream line patterns are no longer axisymmetrical. Especially near the surface of the sphere, the stream lines are moved to those areas in which the smaller viscosity coefficient η_3 is effective.

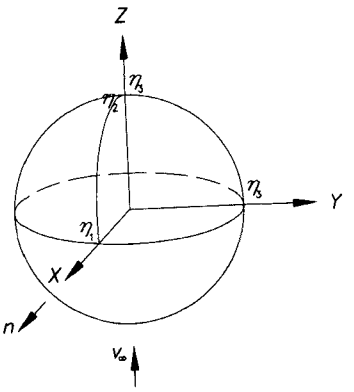

FIGURE 4 Effective viscosity coefficients near the surface of the sphere.

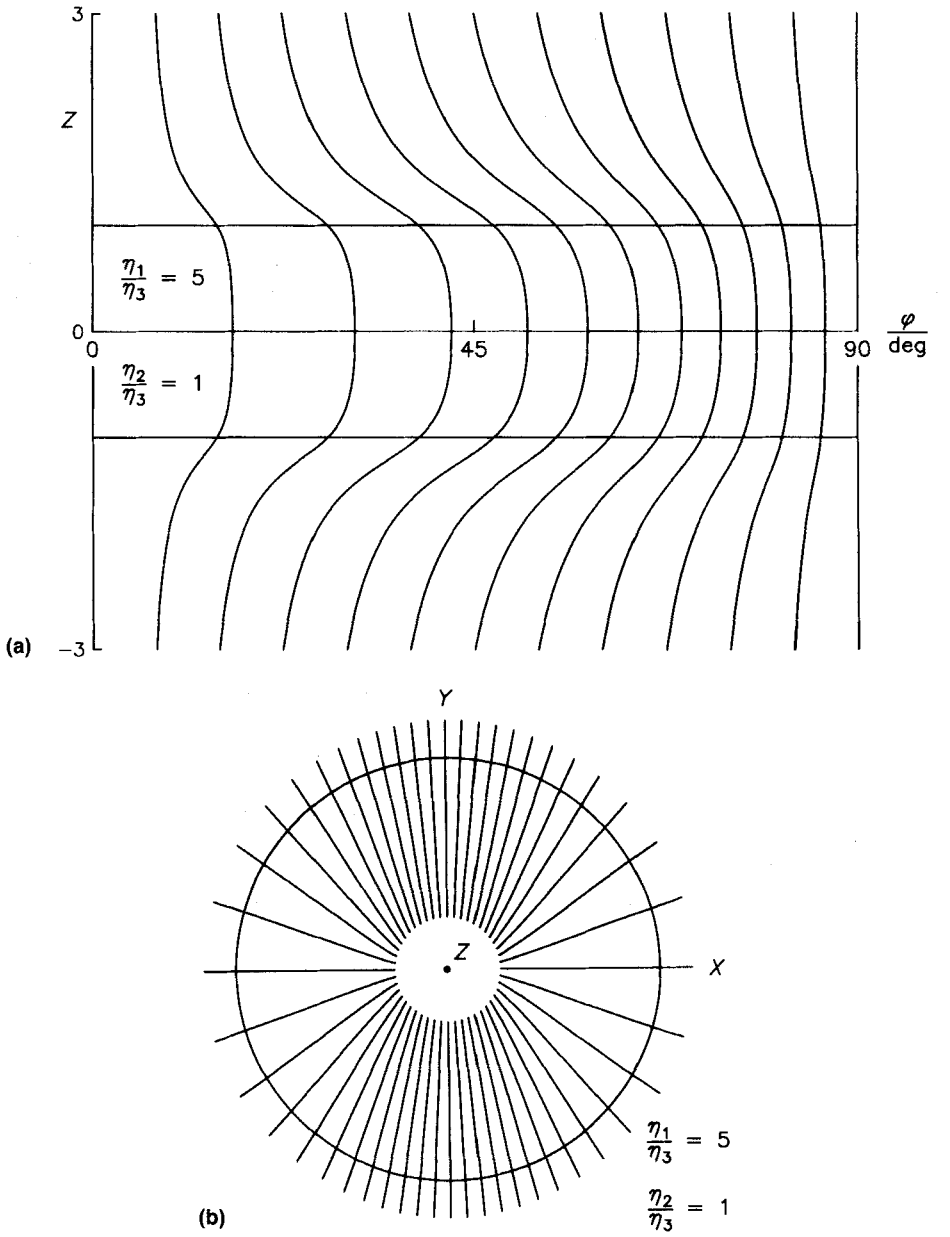

FIGURE 5 Stream line pattern for the flow of a nematic liquid crystal with $\eta_1/\eta_3 = 5$, $\eta_2/\eta_3 = 1$ and $\alpha_1 = 0$ around a fixed sphere. The director is parallel to the x axis and the flow velocity v_∞ at infinite distance is parallel to the z axis.
a) cylinder projection with the coordinates z, ϕ.
b) x, y projection.

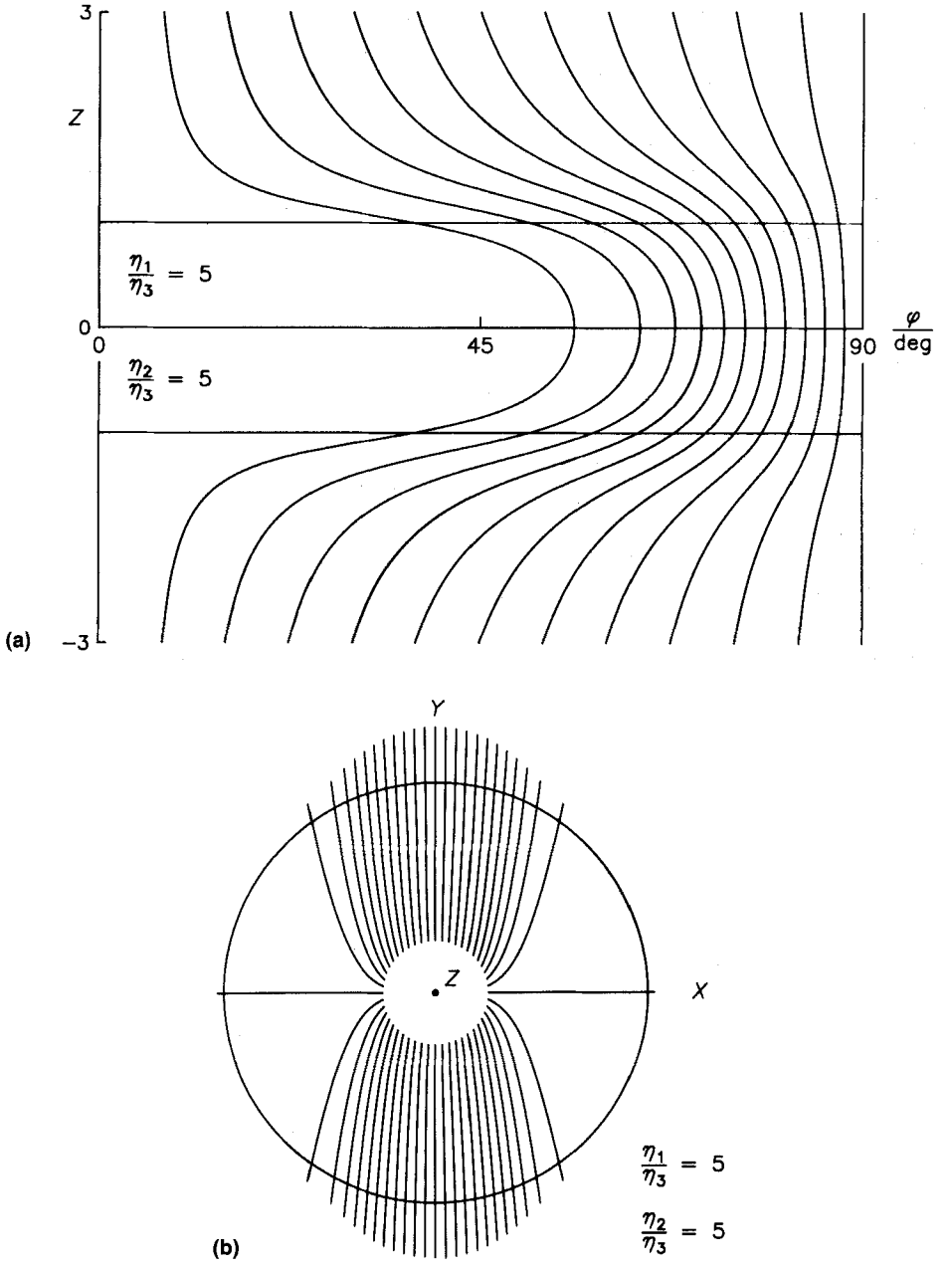

FIGURE 6 Stream line pattern as in Figure 5 for a nematic liquid crystal with $\eta_1/\eta_3 = \eta_2/\eta_3 = 5$ and $\alpha_1 = 0$.

This effect becomes rather strong in Case II, in which the anisotropy causes large viscosity coefficients in the whole x, z plane. Figure 6b shows that the enhanced flow in the y, z plane even leads to stream lines with a larger radius.

Stream line patterns with an oblique director orientation are obtained as follows. The numerical solutions of the hydrodynamic equations are always determined for the cases $v_\infty \parallel z$ and $\boldsymbol{n}$ parallel to the z or the x axis. The solution for the parallel case is now rotated by the angle ψ in the x, z plane and the perpendicular solution is rotated by $90° - \psi$, i.e., the director $\boldsymbol{n} = (\sin\psi, 0, \cos\psi)$ is now parallel for both solutions and the solutions can be superposed such that $v_\infty \parallel z$. The velocities and pressures for this case are obtained by

$$v = \cos\psi\, v_\parallel + \sin\psi\, v_\perp \tag{35}$$

$$p = \cos\psi\, p_\parallel + \sin\psi\, p_\perp \tag{36}$$

In order to get the numerical values for $v_\parallel$, $v_\perp$ and p at the grid points of the reciprocal spherical coordinate system, in which the superposed solution is described, the numerical values have to be interpolated. This was done by a two dimensional (ξ is retained during the rotation) parabolic interpolation using the values at the 9 nearest grid points (biquadratic finite element interpolation). Figure 7 shows a stream line pattern for the case $\boldsymbol{n} = (\sqrt{2}, 0, \sqrt{2})$ and the viscosity coefficient ration $\eta_1/\eta_3 = 5$, $\eta_2/\eta_3 = 1$ and $\alpha_1 = 0$ in the x, z plane. Due to the

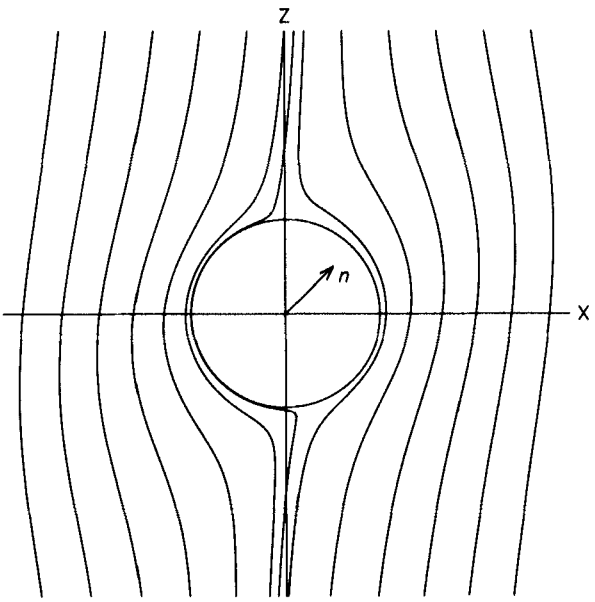

FIGURE 7 Stream line pattern in the x, z plane for the case $v_\infty \parallel z$ and $\boldsymbol{n} = (\sqrt{2},0,\sqrt{2})$ for a nematic liquid crystal with the viscosity coefficient ratio $\eta_1/\eta_3 = 5$, $\eta_2/\eta_3 = 1$ and $\alpha_1 = 0$.

oblique director orientation the stream line pattern is no longer symmetrical to the y, z plane. The flow lines are rotated into the direction of the director which leads to a minimum in the energy dissipation.

The determination of the real pressure requires the knowledge of the Leslie coefficient α_5 (see Equation (34)). We have, therefore, performed the calculation for a liquid crystal for which α_5 is known. The viscosity coefficients of Nematic Phase IV (Merck AG), which is a eutectic mixture of the two isomeric 4-methoxy-4′-n-butylazoxybenzenes, are $\eta_1 = 0.227$, $\eta_2 = 0.0275$, $\eta_3 = 0.0515$ and $\alpha_5 = 0.147$ Pa s.[8] The small influence of the Leslie coefficient α_1 was neglected. Figure 8 shows the modified pressure p'' and the real pressure p in dimensionless form on the surface of the sphere for the x, z and the y, z plane. As for the velocities, the angular dependence of $p = p''$ in the y, z plane is the same as for an isotropic liquid ($p \propto \cos\vartheta$) whereas the dependence on the radius is different. The pressure at $\vartheta = 0$ is considerably higher than for an isotropic liquid (1.5 in dimensionless form) which is due to the small influence of η_2 and the large value of η_1 as compared with η_3 on which the pressure is normalized.

Furthermore, we want to present some results for the force on the sphere. Due to the dependence on three viscosity coefficient ratios (η_1/η_3, η_2/η_3 and α_1/η_3) and to the large computing times, it was not possible to develop an empirical equation as a function of the three viscosity coefficient ratios. Our main interest was the

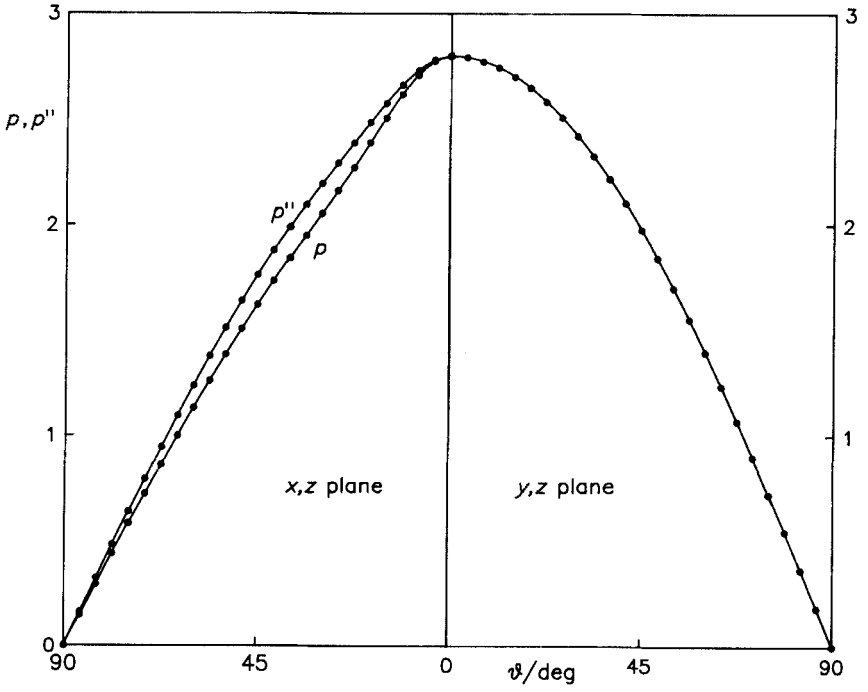

FIGURE 8 Modified pressure p'' and real pressure in dimensionless form on the surface of the sphere in the x, z and the y, z plane for Nematic Phase IV (Merck AG).

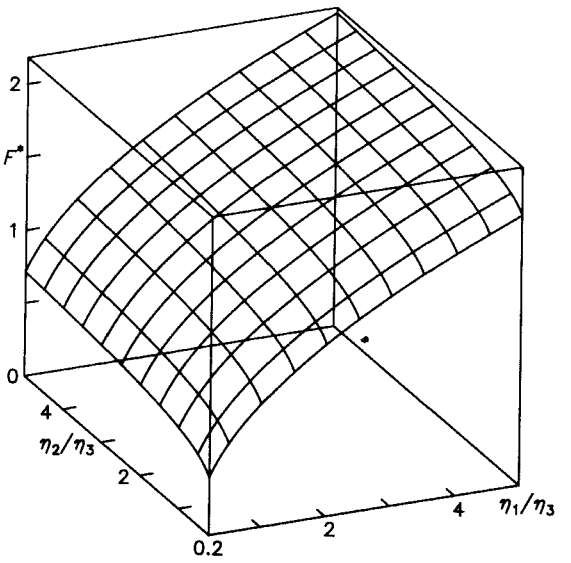

FIGURE 9 Dimensionless force $F^* = F/6\pi\eta_3 R v_\infty$ on the sphere as a function of the viscosity coefficient ratios η_1/η_3 and η_2/η_3 for vanishing α_1 values.

influence of η_1/η_3 and η_2/η_3 on the force for vanishing α_1 values. Figure 9 shows the results which are fitted by the function

$$F^* = a + b\sqrt{\eta_1/\eta_3} + c \ln(\eta_2/\eta_3) + d\sqrt{\eta_1/\eta_3} \ln(\eta_2/\eta_3)$$
$$a = 0.19656, \quad b = 0.8062, \quad c = 0.1007, \quad d = -0.0416 \tag{37}$$

It describes the force within 0.5% if all viscosity coefficient ratios, i.e., also η_1/η_2, are between 0.2 and 5. a is about $1 - b$ as F^* must be one for the isotropic case. Figure 9 shows the very different strength in the dependence on η_1/η_3 and η_2/η_3. The constant d of the coupling term is very small, i.e., the force on the sphere is a nearly additive function of η_1/η_3 and η_2/η_3.

The anisotropy of the viscosity coefficients leads to a perpendicular force on a falling sphere if the director is neither parallel nor perpendicular to the gravitational field. The perpendicular force on the sphere can be calculated from the forces $F_\parallel$ in the axisymmetrical case and $F_\perp$ in the perpendicular case by a superposition analogously to Equations (35) and (36)

$$\mathbf{F} = \cos\psi\, \mathbf{F}_\parallel + \sin\psi\, \mathbf{F}_\perp \tag{38}$$

The numerical calculation was performed for a liquid crystal with $\eta_2 : \eta_3 : \eta_1 : \alpha_1 = 1 : 3 : 10 : 0$. Equation (18) is used for the calculation in the axisymmetrical case which gives

$$\frac{F_\parallel}{\eta_0 R v_0} = 35.7508$$

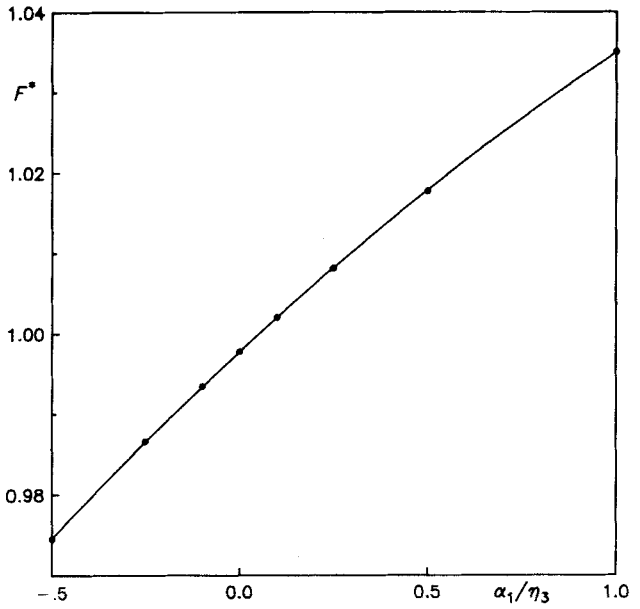

FIGURE 10 Force F^* on the sphere as function of α_1/η for $\eta_1 = \eta_2 = \eta_3 = \eta$.

where v_0 is the velocity of the sphere and η_0 the viscosity coefficient unit. The force $F_\perp$ was determined with the numerical method which gives

$$\frac{F_\parallel}{\eta_0 R v_0} = 89.63$$

Equation (14) from paper I allows to determine the angle β between the falling direction and the gravitational field. We find $\beta = 23.25°$ for $\psi = 45°$ and the maximum angle β is 25.45° for $\psi = 57.7°$.

Finally, we want to present some results for the force on the sphere as a function of α_1. The η coefficients are assumed to be equal ($\eta_1 = \eta_2 = \eta_3 = \eta$). Figure 10 shows the small approximately linear dependence on α_1 which leads to an increase of only 4% for $\alpha_1/\eta = 1$ as compared with the isotropic case. The stability criteria allow negative α_1/η values up to -4. Increasing difficulties with the numeric stability of our numerical procedure did not allow a calculation in this area.

V. CONCLUSION

The finite difference method allows to calculate the force on the sphere for all director orientations and viscosity coefficients. The question arises whether it is

possible to determine the viscosity coefficients from a measurement of the force. The following discussion shows that there are some severe difficulties to overcome.

1) It is assumed in the calculation that the nematic liquid crystal extends up to infinity. For the measurement, it is necessary to use a sample vessel which should exhibit a spherical shape. In this case, the numerical calculations could be performed along the lines discussed above. The displacement of the sphere in the experiment should be so small that the deviation from the concentricity of the spheres is negligible. A calculation shows that this condition leads to problems with the measurement of the force if realistic volumes for the inner and outer sphere are assumed.

2) There are only two independent measurements of the force on the sphere ($v_\infty \parallel \boldsymbol{n}$ and $v_\infty \perp \boldsymbol{n}$) as compared with four unknown viscosity coefficients η_1, η_2, η_3, and α_1 where the influence of the last one can be neglected. Thus, further measurements of the force on bodies with different shape (two and three axial ellipsoids) have to be performed. This would lead to further problems in the numerical calculation procedure.

The discussion shows that it should be advantageous to develop a device in which the torque on a rotating body is measured. Such a device would maintain the concentricity or coaxiality for long times. Due to the small number of independent torque measurements by a variation of the director orientation bodies of different shape have to be used. A convenient system would contain cylinders of different shape (rods, plates, conical shaped bodies) which are rotating in a vessel of corresponding shape. The different shapes and director orientations allow the measurement of η_1, $\eta_1 + \eta_2$, η_3, $\eta_2 + \eta_3$ nearly uninfluenced by the other coefficients. First calculations and experimental tests of such a device are in progress.

Acknowledgment

Financial support by the Deutsche Forschungsgemeinschaft is gratefully appreciated. Our thanks are also due to the Institut für Technische Informatik for computer support on a VAX 6000-410.

APPENDIX

The derivatives in Equations (24–27) in spherical coordinates with a reciprocal radius ξ are

$$\partial_x = \xi \left(-\frac{\sin\phi}{\sin\vartheta}\, \partial_\varphi + \cos\phi \cos\vartheta\, \partial_\vartheta - \xi \cos\phi \sin\vartheta\, \partial_\xi \right) \tag{A1}$$

$$\partial_y = \xi \left(+\frac{\cos\phi}{\sin\vartheta}\, \partial_\varphi + \sin\phi \cos\vartheta\, \partial_\vartheta - \xi \sin\phi \sin\vartheta\, \partial_\xi \right) \tag{A2}$$

$$\partial_z = -\xi(\sin\vartheta\ \partial_\vartheta + \xi\cos\vartheta\ \partial_\xi) \tag{A3}$$

$$\partial_x^2 = \xi^2\left[\frac{\sin^2\phi}{\sin^2\vartheta}\,\partial_\varphi^2 + \cos^2\phi\cos^2\vartheta\,\partial_\vartheta^2 + \xi^2\cos^2\phi\sin^2\vartheta\,\partial_\xi^2\right.$$

$$-\sin 2\phi\cot\vartheta\,\partial_{\vartheta\varphi} + \xi\sin 2\phi\,\partial_{\xi\varphi} - \xi\cos^2\phi\sin 2\vartheta\,\partial_{\vartheta\xi} + \frac{\sin 2\phi}{\sin^2\vartheta}\,\partial_\varphi$$

$$\left.+\left(-\cos^2\phi\sin 2\vartheta + \sin^2\phi\cot\vartheta\right)\partial_\vartheta + \xi\left(-1 + 3\cos^2\phi\sin^2\vartheta\right)\partial_\xi\right] \tag{A4}$$

$$\Delta = \xi^2\left(\frac{1}{\sin^2\vartheta}\,\partial_\varphi^2 + \partial_\vartheta^2 + \xi^2\,\partial_\xi^2 + \cot\vartheta\,\partial_\vartheta\right) \tag{A5}$$

Some of the terms in Equation (A4) can be combined. The errors of the numerical differentiation become, however, larger in this form.

References

1. H. Kneppe, F. Schneider and B. Schwesinger, *Mol. Cryst. Liq. Cryst.*, **205**, 9 (1991).
2. H. Heuer, H. Kneppe and F. Schneider, *Mol. Cryst. Liq. Cryst.*, **200**, 51 (1991).
3. F. M. Leslie, *Arch. Ratl. Mech. Anal.*, **28**, 265 (1968).
4. J. L. Ericksen, *Mol. Cryst. Liq. Cryst.*, **7**, 153 (1969).
5. F. H. Harlow and J. E. Welsh, *Phys. Fluids*, **8**, 2182 (1965).
6. A. J. Chorin, *J. Comp. Phys.*, **2**, 12 (1967).
7. R. Peyret and Th. D. Taylor, Computational methods for fluid flow, Springer 1983, p. 144.
8. H. Kneppe, F. Schneider and N. K. Sharma, *J. Chem. Phys.*, **77**, 3203 (1982).